Fatigue of Engineering Materials and Structures Vol. 5, No. 3, pp. 249–263, 1982
Printed in Great Britain

0160-4112/82/030249-15$03.00/0
Pergamon Press Ltd.

ELASTIC–PLASTIC FINITE ELEMENT ANALYSES OF SHORT CRACKS

WANG TZU CHIANG*
Institute of Mechanics, Academia Sinica, Beijing, China

and

K. J. MILLER
Mechanical Engineering Department, University of Sheffield, U.K.

(*Received in final form* 10 *May* 1982)

Abstract Stress and strain distributions and crack opening displacement characteristics of short cracks have been studied in single edge notch bend and centre cracked panel specimens using elastic–plastic finite element analyses incorporating both a non strain hardening and a power law hardening behaviour. J contour integral solutions to describe stress strain conditions at crack tips for short cracks differ from those for long cracks. The analyses show that (i) short cracks can propagate at stress levels lower than those required for long cracks and (ii) a two-parameter description of crack tip fields is necessary for crack propagation.

Nomenclature

a	Crack length	X, Y	Lagrangian rectangular co-ordinates
b	A unit of length $= 0.27\,J/\sigma_{ys}$	δ_t	Crack tip opening displacement
d_{ij}	Strain rate tensor	$\bar{\epsilon}_p$	Equivalent plastic strain
E	Young's modulus	λ	Single parameter for fracture
J	Rice's path-independent contour integral	μ	Shear modulus
K_I	Mode I stress intensity factor	ν	Poisson's ratio
K_{Ie}	Equivalent stress intensity factor $= \sqrt{\frac{EJ}{(1-\nu^2)}}$	σ_e	Equivalent stress
		σ_{ij}	Cauchy stress tensor
L	Specimen length	σ_M	Bending stress $= \frac{6PL}{4(W-a)^2}$
P	Load		
r, θ	Polar co-ordinates	σ_0	Hydrostatic stress $= (\sigma_1 + \sigma_2 + \sigma_3)/3$
S_x, S_y, S_z	Stress deviator	σ_{ys}	Yield stress in uniaxial tension
U_y	Crack face displacement	σ_θ	Circumferential stress
V_i	Velocity rate vector	σ_z	Through thickness stress
W	Specimen width		

INTRODUCTION

CRACK BIRTH in components usually begins at a very small surface defect or the root of a notch or second phase particle. When such a crack is born, it will be a very short crack [1].

Much work has been published concerning large scale plastic deformation of long cracks. McClintock [2] and Rice and Johnson [3] have studied slip-line configurations

* Currently at the University of Sheffield, U.K.

around cracks and notches. McMeeking [4] and McMeeking and Parks [5] have shown that finite strain effects are important over a distance of about 2 or 3 times the crack opening displacement. Shih [6] calculated the crack opening displacement and found a relationship between COD and the J-integral. But all of these studies were concerned with long cracks. Now short cracks in fatigue exhibited a different crack growth behaviour than long cracks [7]. Hammouda and Miller [8] have pointed out that short cracks will grow even below the threshold stress intensity factor range $\Delta K_{I\text{th}}$. This type of behaviour requires to be quantified in mechanical terms and hence the present work outlines in detail the stress and strain fields for short cracks.

Short cracks differ from long cracks either because (i) the net section stresses are so high that they exceed $0.4\,\sigma_{ys}$ and the crack tip plastic zones are so large that LEFM parameters do not characterize the elastic–plastic stress field ahead of the crack with sufficient accuracy; or (ii) the crack itself is so small, say less than 0.25 mm [9] that LEFM parameters cannot quantify the fracture process zone at the crack tip. This typically occurs when a crack is embedded in a single crystal on the surface of a body.

This paper examines short cracks for case (i) above and compares solutions with those obtained on long cracks. Using a finite element method based on finite strain formulation of plastic flow theory, one can obtain the complete stress and strain fields. Fracture criteria, based on a combination of critical stress or strain, are then discussed for crack initiation. In addition, fatigue crack growth for short cracks is discussed in relation to the plastic zone and the plastic strain field.

ANALYSES

The variational equations presented in [10] and [11] are,

$$\delta U = \int_V \mathbf{f}^{(1)} \cdot \tilde{\mathbf{V}}\, \mathrm{d}V + \int_{S_\sigma} \mathbf{p}^{(1)} \cdot \tilde{\mathbf{V}}\, \mathrm{d}s, \tag{1}$$

and

$$U = \frac{1}{2} \cdot \int_V \left\{ 2\mu \left[d_{ij} \cdot d_{ij} - \frac{\nu}{(1-2\nu)} \cdot (d_{kk})^2 - \frac{\alpha}{g^*} (N_{ij} \cdot d_{ij})^2 \right] - \sigma_{ij}(2d_{ik}d_{jk} - V_{k,i}V_{k,j}) \right\} \mathrm{d}V, \tag{2}$$

where

$\tilde{\mathbf{V}}$ = the virtual velocity fields,
$\mathbf{f}^{(1)}$ = the convected derivative of the body force vector,
$\mathbf{p}^{(1)}$ = the convected derivative of the surface force vector,
N_{ij} = the non-dimensional Cauchy stress deviator,
$N_{ij} = S_{ij}/\sqrt{S_{kl} \cdot S_{kl}}$,
S_{ij} = the Cauchy stress deviator,
$g^* = 1 + A'(\bar{\epsilon}_p)/3\mu$,
$A'(\bar{\epsilon}_p)$ = $\mathrm{d}A(\bar{\epsilon}_p)/\mathrm{d}\bar{\epsilon}_p$ where $A(\bar{\epsilon}_p)$ is the scalar function which characterizes the plastic stress–strain relation.

$$\alpha = \begin{cases} 1; & \text{at } \bar{\sigma}_e = A(\bar{\epsilon}_p) \text{ and } N_{ij}d_{ij} > 0 \\ 0; & \text{at all other conditions.} \end{cases}$$

Equation (1) is equivalent to the equilibrium equations of stress rate fields for large deformation theory employing up-dated Lagrangian co-ordinates. The finite element analyses are based on equation (1). Eight-noded isoparametric elements with 3 by 3 Gauss points are employed in the calculations for centre cracked panels (CCP) and single edge notched bend (SENB) type specimens. The material behaviour is modelled by a power-law relationship of the form,

$$\sigma_e = \sigma_{ys}(\bar{\epsilon}_p/\bar{\epsilon}_{po})^n \tag{3}$$

where σ_e is the equivalent stress, σ_{ys} is the yield stress, $\bar{\epsilon}_p$ is the equivalent plastic strain and $\bar{\epsilon}_{po}$ is the equivalent plastic strain at first yield.

The calculation uses an incremental tangent modulus procedure and contains approximately 200–300 load increments.

The finite element mesh

The finite element mesh employed is shown in Fig. 1 in its undeformed configuration. In zone C the 8 elements connected to the crack tip are degenerated to triangular elements. The smallest length of the elements at the crack tip range between 0.0005 ~ 0.001 mm which is only 5–10% of the short crack length of 0.01 mm. The a/W ratio is 0.005.

The total mesh contains 398 nodes and 115 plane strain isoparametric elements. For the three point bend specimen only one half of the specimen is used because of symmetry. For the centre cracked panel, only one quarter of the specimen is used. The mesh is

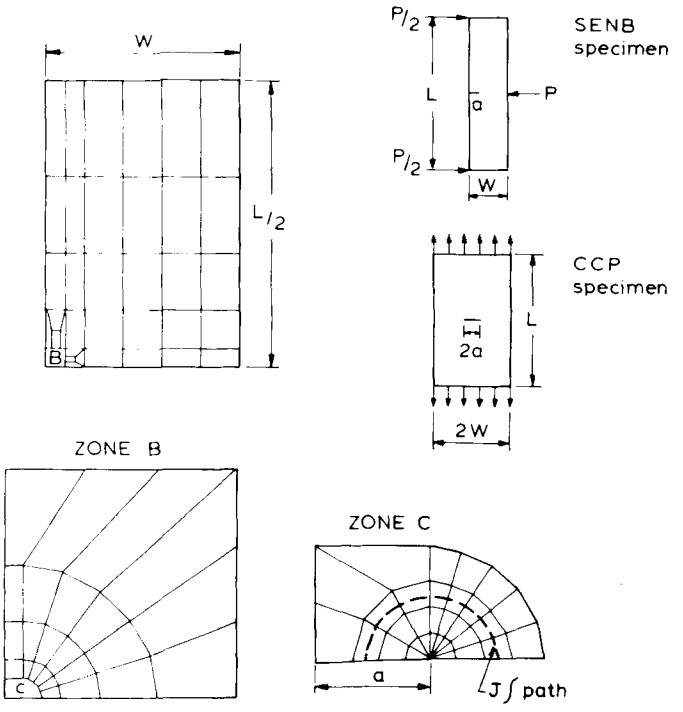

Fig. 1. SENB and CCP specimen configurations together with finite element idealization.

formed automatically and the mesh can be easily changed. Also shown in Fig. 1 is the J integral path.

Results

Calculations were carried out for plane strain conditions and both a non-hardening and a power-law hardening material. Material properties were $\nu = 0.3$ and $\sigma_{ys}/E = 1/300$. For the power-law hardening material the hardening coefficient n was made equal to 0.2. All results are expressed in the Lagrangian co-ordinates (X, Y), of the undeformed configuration.

Crack profile and blunted-tip shapes

As the load increases, the sharp crack will first become a very narrow slit and then progressively blunted. Crack profiles for a hardening material are shown in Fig. 2 for (a) SENB and (b) CCP specimens respectively.

Generally speaking, the crack profile contains an inclined but straight face for the three point bend specimen at low stresses that is similar to long cracks. One can visualize this inclined face to be obtained by rotating the crack faces around a centre some distance ahead of the crack. At higher stresses, equivalent to short cracks, this straight face is reduced in length. For the centre cracked panel, the crack face profiles are more akin to ellipses.

In this study the crack tip opening displacement, δ_t, is taken at the intercepts of the two 45° lines drawn back from the tip of the deformed profile, see Fig. 3, which shows that the blunted crack tip shape for hardening materials is similar to the results of McMeeking [4], but there are some differences. The blunted crack tip shape of a long crack is more like a half circle but for the short crack the opening displacement increases more rapidly on the flank.

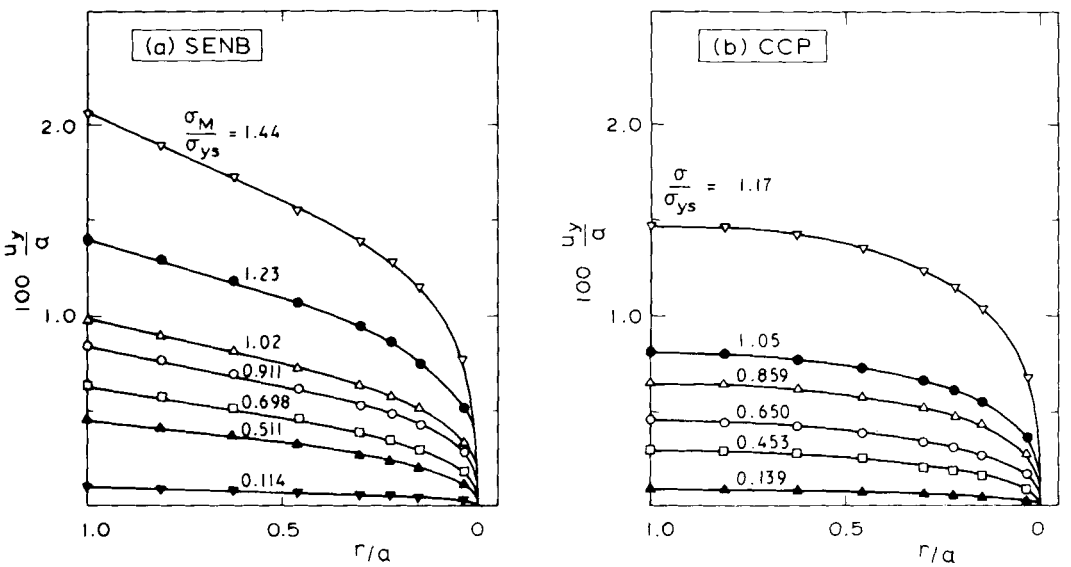

Fig. 2. Crack profiles for a hardening material: (a) SENB specimen; (b) CCP specimen.

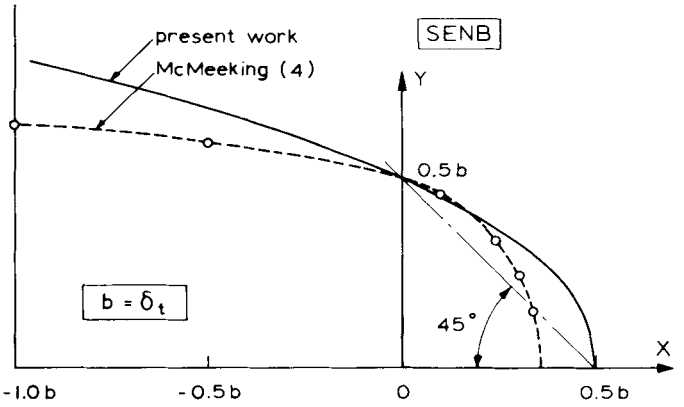

Fig. 3. Blunted crack tip profiles for a hardening material.

Using the expression

$$\delta_t = \alpha \cdot J/\sigma_{ys} \tag{4}$$

McMeeking shows that for $\sigma_{ys}/E = 1/300$ and $n = 0.2$, the value of α is 0.27 whilst for the present work $\alpha = 0.264$.

Plastic zones

As the load increases, the plastic zone develops around the crack tip; see Figs 4 and 5. When the equivalent stress intensity factor

$$K_{Ie} = \sqrt{\frac{EJ}{1-\nu^2}}$$

is 4.12 MN m$^{-3/2}$ the plastic zone size is about 1.5 times the crack length for the SENB specimen. When the value of K_{Ie} is equal to 7.22 MN m$^{-3/2}$ the plastic zone size is projected back to the free boundary AB.

For the CCP specimen, the plastic zone develops more rapidly as compared to the SENB specimen. When the value of K_{Ie} is equal to 3.69 MN m$^{-3/2}$, the plastic zone size is about 2 times the crack length. The plastic zone will surround the whole crack in a CCP specimen at $K_{Ie} = 4.34$ MN m$^{-3/2}$ as shown in Fig. 5. When plasticity is so extensive it will not be possible for the J integral to characterize the behaviour of short cracks.

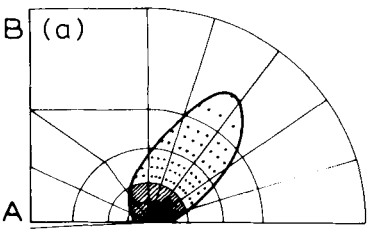

Fig. 4(a)

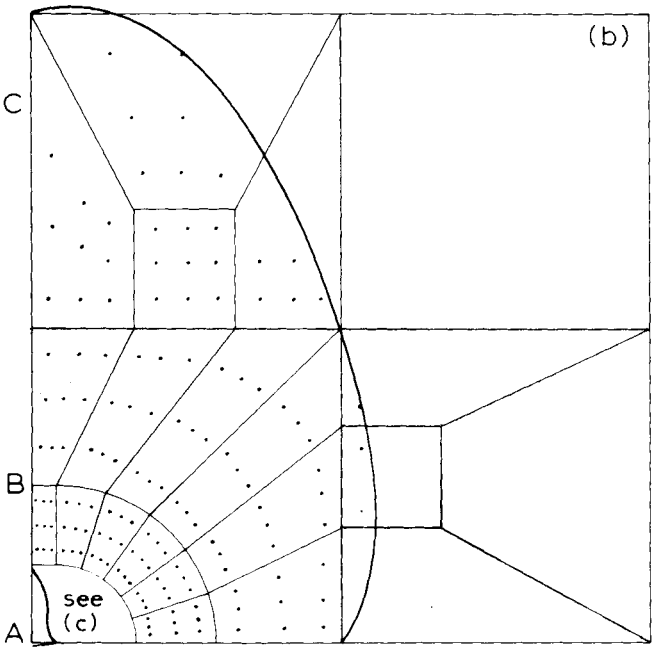

Fig. 4(b).

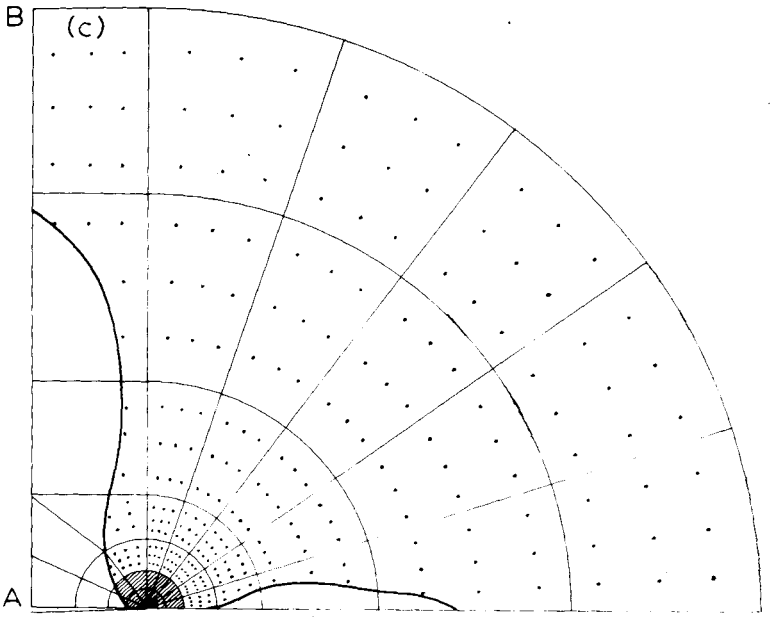

Fig. 4(c).

Fig. 4. Plastic zone shapes for a SENB specimen and a hardening material. Note the hatched area is plastically deformed but is too small to show the integration points: (a) $K_{Ie} = 4.12\ \text{MN m}^{-3/2}$; (b) $K_{Ie} = 7.22\ \text{MN m}^{-3/2}$; (c) Enlargement of (b) close to the crack tip.

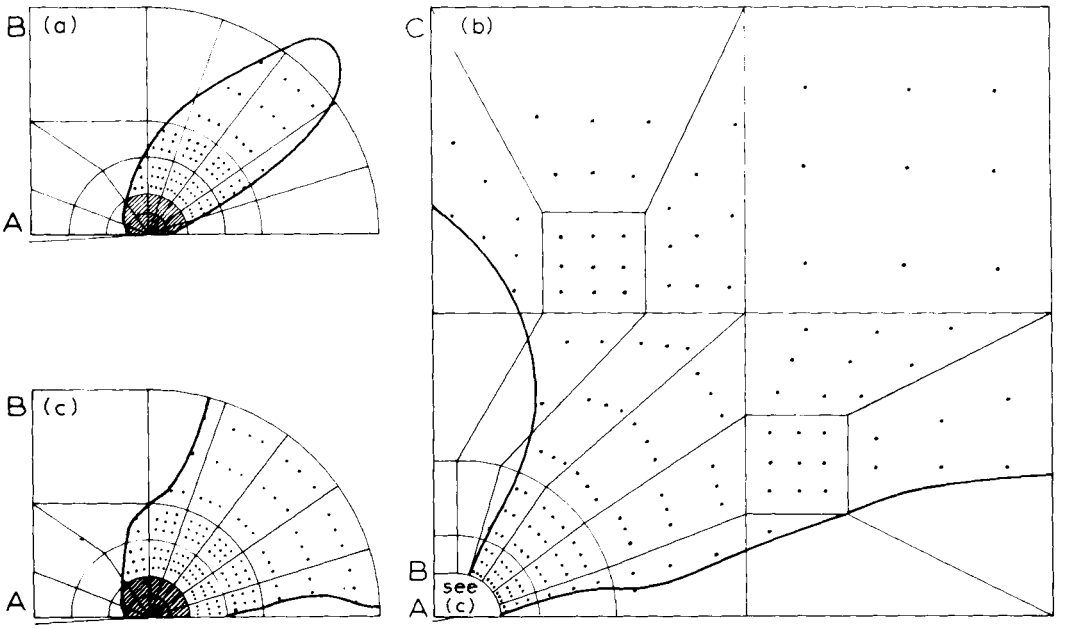

Fig. 5. Plastic zone shapes for a CCP specimen and a hardening material. Note the hatched area is plastically deformed but too small to show the integration points: (a) $K_{Ie} = 3.69\ \text{MN m}^{-3/2}$; (b) $K_{Ie} = 4.34\ \text{MN m}^{-3/2}$; (c) enlargement of (b) close to the crack tip.

Stress and plastic strain distribution at the crack tip

In Fig. 6(a), the true stress σ_θ is plotted against the distance from the crack tip for a hardening material. The distance is normalized by the J-integral. The dashed lines are the small scale yielding results for the long crack obtained by McMeeking [4]. The solid lines are derived from the present work. It is clear that when $r/b < 1$, our results are higher than those of McMeeking. This is because McMeeking did not analyse a sharp crack but studied a narrow slit, therefore the hydrostatic stress could not be maintained at the notch-like surface. However when $r/b > 1$, the value of σ_θ for a short crack is lower than those given by McMeeking.

The equivalent plastic strain $\bar{\epsilon}_p$ is shown in Fig 6(b). The results for the short crack are higher than for the long crack, when $r/b > 1$. This cannot be attributed to different boundary conditions between the narrow slit employed by McMeeking and a sharp crack tip. In fact, using a narrow slit instead of a sharp crack will cause a decrease in hydrostatic stress and hence increase the plastic strain $\bar{\epsilon}_p$. The main reason why the plastic strain is higher for a short crack, is because the plastic zone size itself is large. As previously mentioned, when the $K_{Ie} = 7.22\ \text{MN m}^{-3/2}$, the plastic zone size is projected back to the free boundary AB and is about 9 times the crack length and so crack tip plastic flow is enchanced.

According to the J integral theory, plots of the stress distributions near the crack tip versus $X/(J/\sigma_{ys})$ should be independent of geometrical configuration and load level. This is nearly true for the SENB specimen and a long crack, but this is not the case for a short crack. The relation between stress ratio $\sigma_\theta/\sigma_{ys}$ and nondimensional distance $X(J/\sigma_{ys})$ is shown in Fig. 7 for various loading levels. It is seen that the stress distributions are

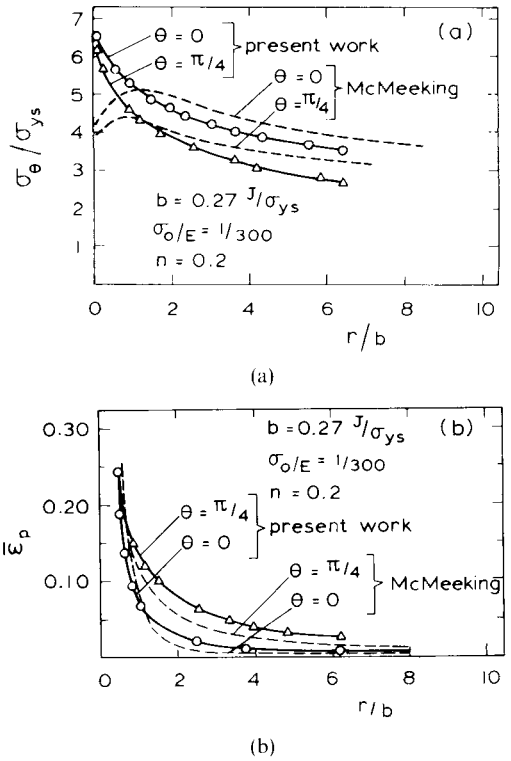

Fig. 6. Stresses and strains at a crack tip in an SENB specimen and a hardening material as a function of non-dimensional distance from the crack tip when $a.\sigma_{ys}/J = 76.4$: (a) stress ratio $\sigma_\theta/\sigma_{ys}$; (b) equivalent plastic strains.

dependent on geometrical configuration and loading level. As the value of J increased, the deviation from the small scale yielding results for the long crack became more distinct.

In Fig. 8 the true stress σ_θ is plotted against K_{Ie} (equivalent to the J-integral) for $\theta = 0$. It is clear, that the stress σ_θ for the bend specimen is higher than the centre cracked panel. This is because the bend specimen has a higher triaxial stress. When K_{Ie} is low the stress distribution is not geometry dependent but at higher values of K_{Ie} this is not the case.

The relations between stresses and strains for a hardening material are shown in Fig. 9. The curves are very similar to uniaxial tension curves. As the plastic strain $\bar{\epsilon}_p$ increases, the stress will increase and at some point will reach a maximum value before gradually decreasing with intense plastic strain. In this figure, stresses are also shown as a function of normal strain ϵ_θ.

In Fig. 10, the stresses σ_z, σ_0 are plotted against $\bar{\epsilon}_p$ for a hardening material. According to perfect plasticity theory, the hydrostatic stress σ_0 is equal to σ_z for the plane strain problem. Because perfect plasticity theory ignores elastic deformation, for the general case of an elastic–plastic material differences are observed. However the present work shows that, not only for a non-hardening material but also a hardening material, the triaxial stress σ_0 is nearly identical to σ_z at large plastic strains.

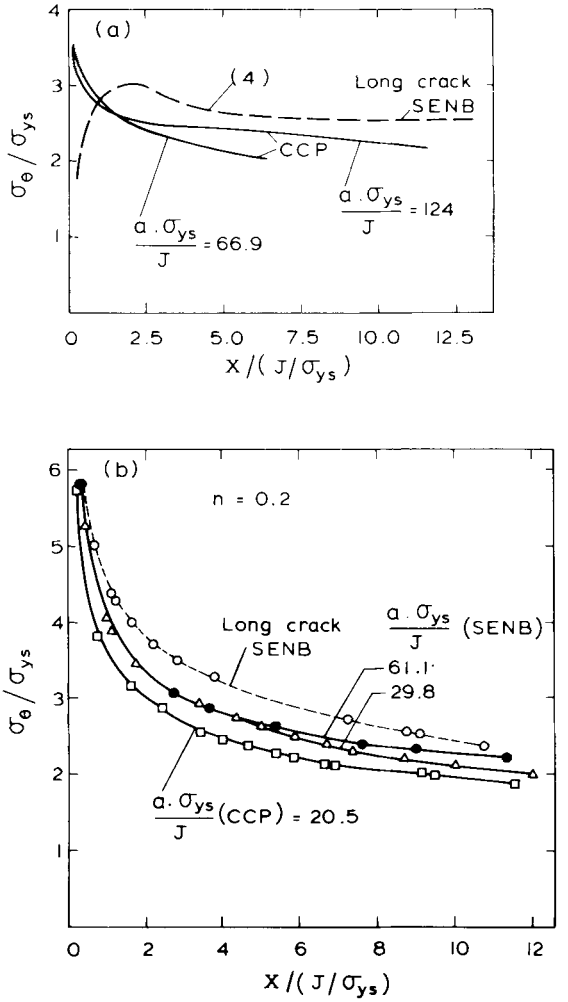

Fig. 7. Stress ratio $\sigma_\theta/\sigma_{ys}$ vs $X.\sigma_{ys}/J$ at $\theta = 0$: (a) a non-hardening material; (b) a hardening material.

The normal stress σ_θ and shear stress $\tau_{r\theta}$ in the direction of $\theta = 56°$ is plotted against the plastic strain $\bar{\epsilon}_p$ in Fig. 11. The maximum shear stress is an important parameter for fatigue crack initiation and growth and it should also be noted that in the final stages of ductile fracture, rupture usually occurs in a direction of maximum shear stress. For the short crack the maximum shear stress $(\tau_{r\theta})_{max}$ in the present study occurs when $\theta = 56°$.

However in Fig. 12(a) where the normal stresses σ_θ, σ_z and σ_r at $\theta = 45°$ are plotted vs the plastic strain $\bar{\epsilon}_p$ it is remarkable that all normal stresses are nearly identical at large plastic strains which indicates that this plane also is the plane of maximum shear stress. It follows that on planes not inclined at 45° (see Fig. 12(b) where $\theta = 56°$) to the crack tip, the maximum shear planes are not coincident. For example the maximum value of shear stress is at $\theta = 56°$; but the radial plane is not the plane of maximum shear. Hence the plane, $\theta = 45°$, may be more important in fatigue crack growth than the plane $\theta = 56°$.

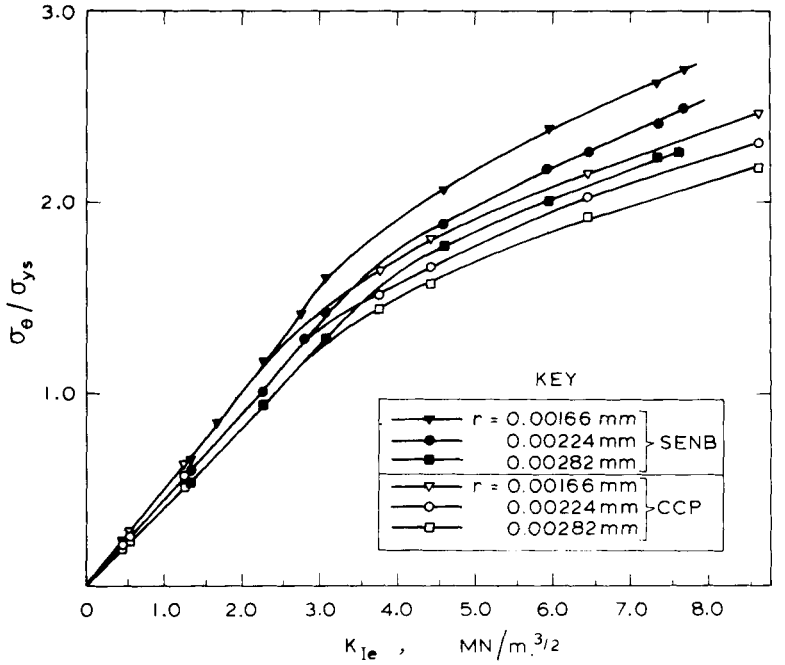

Fig. 8. Stress ratio $\sigma_{\theta\theta}/\sigma_{ys}$ vs equivalent stress intensity factor for a hardening material.

Figure 13 shows the true stress at the crack tip as load increases for both a long and a short crack. This indicates that the J contour integral can not uniquely define the stress at the tip of short cracks. In this figure the a/W ratio is 0.5 and 0.005 for the long and short crack respectively.

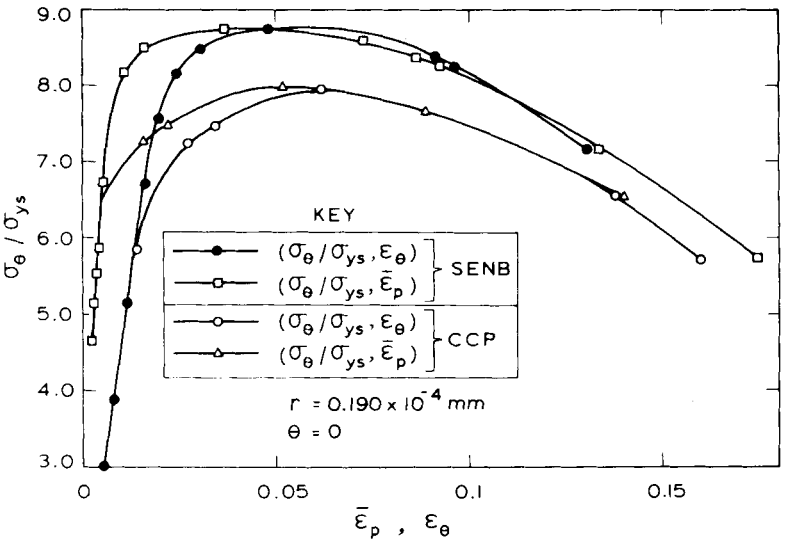

Fig. 9. Crack tip stress/strain relations of a hardening material.

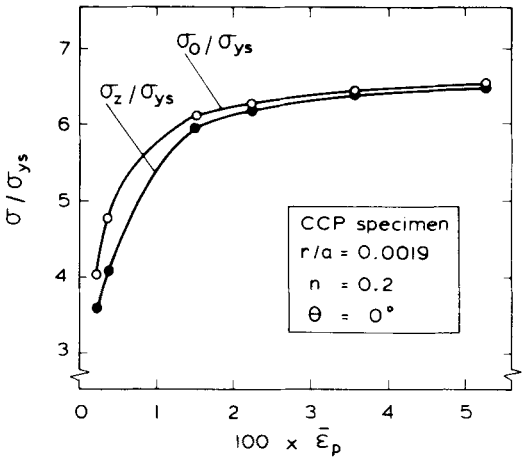

Fig. 10. Relationships of σ_0/σ_{ys} and σ_z/σ_{ys} with strain at $\theta = 0$ for a hardening material.

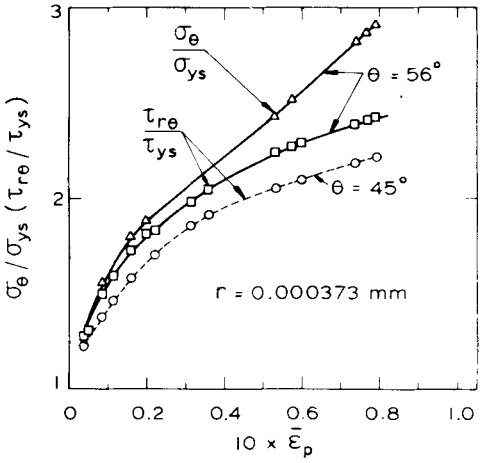

Fig. 11. Stress ratios $\sigma_{\theta\theta}/\sigma_{ys}$ and $\tau_{r\theta\theta}/\sigma_{ys}$ vs equivalent plastic strain for a hardening material and a CCP specimen at $\theta = 56°$ when $r = 0.000373$ mm. The dashed line gives the shear-stress at 45° for the same load.

FRACTURE CRITERIA

Single parameter criteria

From a micromechanics viewpoint, fracture criteria should be solidly based on realistic physical models which simulate the relevant fracture mechanisms. However, the development of quantitative fracture analyses based on micromechanisms is difficult. The study of fracture mechanics therefore aims to describe the stresses and strains in the vicinity of a crack tip and also to provide fracture criteria accounting for different fracture mechanisms if at all possible.

For a long time, a single parameter such as J or δ has been most attractive. However, after intensive investigation, no single parameter is universally applicable. The J-integral

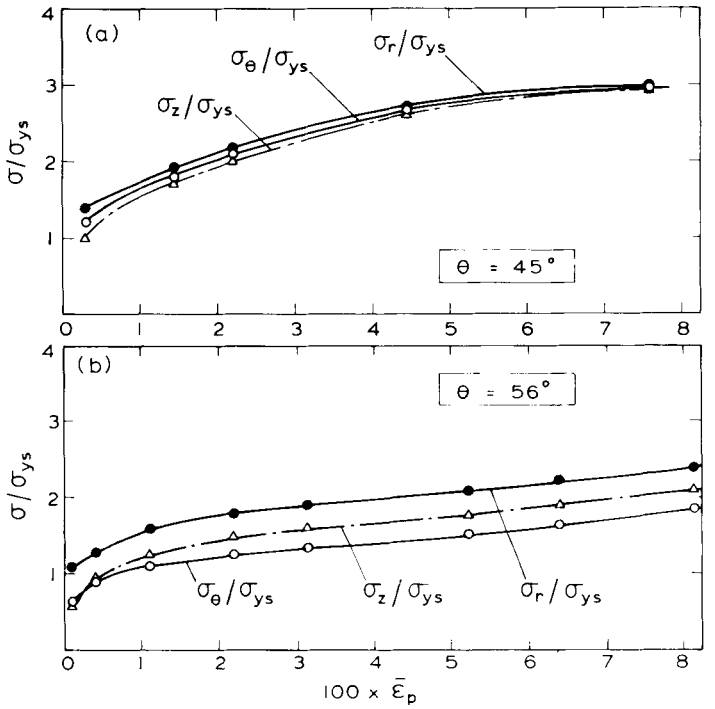

Fig. 12. Comparison of crack tip stress ratios as plastic strain increases in a CCP specimen and a hardening material when r/a = 0.0373: (a) $\theta = 45°$; (b) $\theta = 56°$.

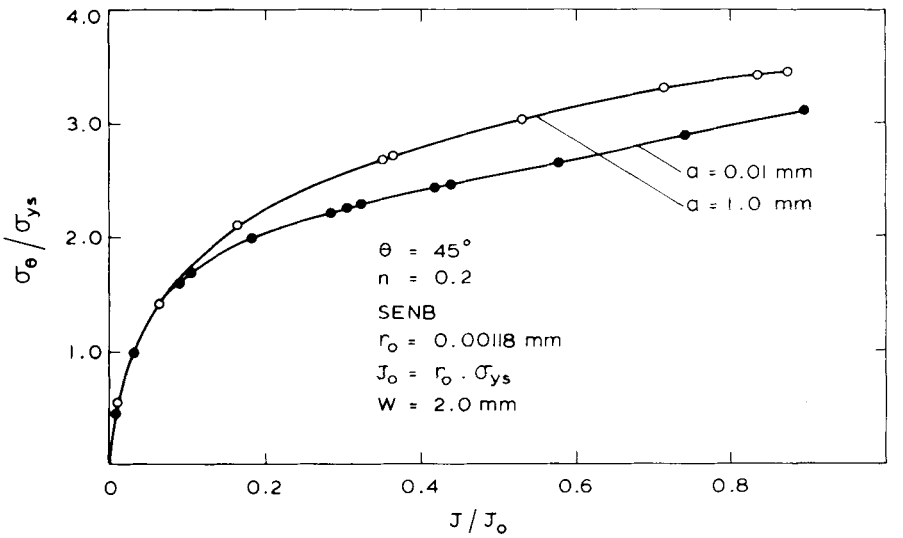

Fig. 13. True stresses ahead of a crack tip as a function of J integral.

and crack tip opening displacement δ_t are useful with certain restrictions, but the restrictions include a strong function of the specimen configuration and the loading system that induces large scale yielding.

It is clear that one single parameter is not sufficient to characterize the crack tip stress–strain fields, e.g. [12, 13]. Indeed if there was a single parameter λ that could characterize the crack tip fields, one could arrive at the relation:

$$\sigma_{ij} = f_{ij}(r, \theta; \lambda), \tag{5}$$

$$\epsilon_{ij} = g_{ij}(r, \theta; \lambda), \tag{6}$$

$$\bar{\epsilon}_p = h(r, \theta; \lambda). \tag{7}$$

The functions, f_{ij}, g_{ij} and h should be independent of geometrical configuration and loading condition but because the plastic strain $\bar{\epsilon}_p$ is always increasing with λ increasing it follows that:

$$\lambda = H(r, \theta; \bar{\epsilon}^*_p); \quad \text{when } r = r_0, \theta = 0, \lambda = H(\bar{\epsilon}^*_p). \tag{8}$$

The function H is dependent on r_0 and one can choose any value of r_0 in the dominant region. For a given r_0, the function H should be uniquely defined.

Here $\bar{\epsilon}^*_p$ is the plastic strain $\bar{\epsilon}_p$ at $r = r_0$ and $\theta = 0$. Substituting equation (8) into equations (5) and (6) one obtains:

$$\sigma_{ij} = F_{ij}(r, \theta; \bar{\epsilon}^*_p), \tag{9}$$

$$\epsilon_{ij} = G_{ij}(r, \theta; \bar{\epsilon}^*_p). \tag{10}$$

The functions of F_{ij} and G_{ij} are, therefore, independent of specimen geometry and loading manner. From the above expressions one can conclude that the plastic strain $\bar{\epsilon}^*_p$ is also a single parameter which can characterize the crack tip fields. However, according to the present work this is not true for large scale yielding. So there is no single parameter which can dominate the crack tip stress–strain fields.

Two parameter criteria

Several investigators have proposed two parameter criteria, Mackenzie, Hancock and Brown [14] proposed the critical plastic strain $\bar{\epsilon}_f$ criterion, where the critical strain $\bar{\epsilon}_f$ is dependent on the stress state which can be characterized by a second parameter σ_0/σ_e. Here σ_e is the equivalent stress and σ_0 is the triaxial stress. They carried out a series of experiments to determine the relation between $\bar{\epsilon}_f$ and σ_0/σ_e.

Generally speaking, ductile fracture involves three distinct processes: void nucleation, void growth and finally coalescence between voids. All of these processes are governed by plastic deformation. As pointed out by McClintock [2] the triaxial stress has very important effects on void growth. Furthermore, Thomason's [15] theory reveals that triaxial stress plays an important role in the microscopic necking between voids. So it is reasonable to choose plastic strain $\bar{\epsilon}_p$ and either ratio σ_0/σ_{ys} or σ_0/σ_e as the two parameters to represent fracture behaviour. The present work shows some features of these two parameters. From Fig. 10 once can conclude that the stress deviator S_z is approximately equal to zero at $\theta = 0$ because the normal stress σ_z is nearly identical with the

triaxial stress σ_0. On the crack line:

$$\left.\begin{aligned} S_z &= 0, \\ \tau_{xy} &= 0, \\ S_y = S_x &= \frac{\sigma_e}{\sqrt{3}} \end{aligned}\right\} \tag{11}$$

$$\left.\begin{aligned} \sigma_x &= S_x + \sigma_0 \\ \sigma_y &= S_y + \sigma_0 \end{aligned}\right\}. \tag{12}$$

Since the equivalent stress σ_e can be directly determined from the equivalent plastic strain $\bar{\epsilon}_p$ it is clear that the stress state at $\theta = 0^\circ$ can be described by the two parameters $\bar{\epsilon}_p$ and σ_0. It can be seen from Fig. 12 that the stresses σ_θ, σ_z, σ_0 are nearly identical at $\theta = 45^\circ$ for large plastic strains $\bar{\epsilon}_p$. Hence, the stress state at $\theta = 45^\circ$ can also be described by the two parameters σ_0 and $\bar{\epsilon}_p$.

If crack initiation is due to coalescence between a main crack and voids along the line $\theta = 0$, then one can choose σ_0, $\bar{\epsilon}_p$ at which $\theta = 0$ as the two governing parameters. However, if crack initiation is due to decohesion or void coalescence along the plane $\theta = 45^\circ$, then one can choose σ_0 and $\bar{\epsilon}_p$ at $\theta = 45^\circ$ as the two governing parameters.

CONCLUSIONS

1. The plastic zone develops rapidly at short cracks and local plastic flow is much easier than in the case of long cracks.
2. The equivalent plastic strain for a short crack is greater than the equivalent plastic strain of a long crack at the same value of the equivalent stress intensity factor. This is why a short fatigue crack will grow below the threshold stress intensity factor determined from experiments on long cracks.
3. A single parameter is not sufficient to characterize crack tip stress–strain fields.
4. The plane radiating at $\theta = 45^\circ$ from the crack tip is the plane of maximum shear stress but $(\tau_{r\theta})_{max}$ occurs when $\theta = 56^\circ$.

REFERENCES

1. Miller, K. J. (1982) The short crack problem. *Fatigue Engng Mater. Struct.* **5**, 229–238.
2. McClintock, F. A. (1968) A criterion for ductile fracture by the growth of holes. *J. appl. Mech.* **35**, 363–371.
3. Rice, J. R. and Johnson. M. A. (1970) The role of large crack tip geometry changes in plane strain fracture. In *Inelastic Behaviour of Solids*, (Kanninen, M. F. *et al.*, Eds) McGraw-Hill, pp. 641–672.
4. McMeeking, R. M. (1977) Finite deformation analysis of crack-tip opening in elastic-plastic materials and implications for fracture. *J. Mech. Phys. Solids* **25**, 357.
5. McMeeking, R. M. and Parks, D. M. (1979) On criteria for J-Dominance of crack tip fields in large scale yielding. ASTM STP 668, pp. 175–194.
6. Shih, C. F. (1979) Relationships between the J-integral and the crack opening displacement for stationary and extending cracks. General Electric Company TIS Report, 79CRDO75.
7. Lankford, J. (1982) The growth of small fatigue cracks in 7075–T6 aluminium. *Fatigue Engng Mater. Struct* **5**, 239–254.
8. Hammouda, M. M. and Miller, K. J. (1979) Elastic plastic fracture mechanics analyses of notches. ASTM STP 668, pp. 703–719.

9. Smith, R. A. (1977) On the short crack limitations of fracture mechanics. *Int. J. Fract.* **13**, 717–719.
10. McMeeking, R. M. and Rice, J. R. (1975) Finite element formulations of large elastic-plastic deformation. *Int. J. Solids Struct.* **11**, 601–616.
11. Wang, T. C. (1981) Fundamental equations for large plastic deformation and finite element formulations. Special issue of *Acta Mechanica Sinica*, pp. 182–192.
12. Miller, K. J. (1977) Fatigue under complex stress. *Metal Sci.* **11**, 432–438.
13. Miller, K. J. and Kfouri, A. P. (1979) A comparison of elastic-plastic fracture parameters in biaxial stress states. ASTM STP 668, pp. 214–228.
14. MacKenzie, A. C., Hancock J. W. and Brown, D. K. (1977) On the influence of state of stress on ductile failure initiation in high strength steels. *Engng Fract. Mech.* **9**, 167.
15. Thomason, P. F. (1968) A theory for ductile fracture by internal necking of cavities. *J. Inst. Metals* **96**, 360.